journal homepage: www.intl.elsevierhealth.com/journals/cmpb

Automated diagnosis of macular edema and central serous retinopathy through robust reconstruction of 3D retinal surfaces

Adeel M. Syed [a], *Taimur Hassan* [b,*], *M. Usman Akram* [c], *Samra Naz* [c], *Shehzad Khalid* [d]

[a] *Department of Software Engineering, Bahria University, Islamabad, Pakistan*
[b] *Department of Electrical Engineering, Bahria University, Islamabad, Pakistan*
[c] *Department of Computer Engineering, National University of Sciences and Technology, Islamabad, Pakistan*
[d] *Department of Computer Engineering, Bahria University, Islamabad, Pakistan*

ARTICLE INFO

Article history:
Received 3 May 2016
Accepted 7 September 2016

Keywords:
Optical coherence tomography
Medical image analysis
Structure tensor
Macular edema (ME)
Central serous retinopathy (CSR)
Retinal surfaces

ABSTRACT

Background and objectives: Macular diseases tend to damage macula within human retina due to which the central vision of a person is affected. Macular edema (ME) and central serous retinopathy (CSR) are two of the most common macular diseases. Many researchers worked on automated detection of ME from optical coherence tomography (OCT) and fundus images, whereas few researchers have worked on diagnosing central serous retinopathy. But this paper proposes a fully automated method for the classification of ME and CSR through robust reconstruction of 3D OCT retinal surfaces.

Methods: The proposed system uses structure tensors to extract retinal layers from OCT images. The 3D retinal surface is then reconstructed by extracting the brightness scan (B-scan) thickness profile from each coherent tensor. The proposed system extracts 8 distinct features (3 based on retinal thickness profile of right side, 3 based on thickness profile of left side and 2 based on top surface and cyst spaces within retinal layers) from 30 labeled volumes (10 healthy, 10 CSR and 10 ME) which are used to train the supervised support vector machines (SVM) classifier.

Results: In this research we have considered 90 OCT volumes (30 Healthy, 30 CSR and 30 ME) of 73 patients to test the proposed system where our proposed system correctly classified 89 out of 90 cases and has promising receiver operator characteristics (ROC) ratings with accuracy, sensitivity and specificity of 98.88%, 100%, and 96.66% respectively.

Conclusion: The proposed system is quite fast and robust in detecting all the three types of retinal pathologies from volumetric OCT scans. The proposed system is fully automated and provides an early and on fly diagnosis of ME and CSR syndromes. 3D macular thickness surfaces can further be used as decision support parameter in clinical studies to check the volume of cyst.

© 2016 Elsevier Ireland Ltd. All rights reserved.

* *Corresponding author.* Department of Electrical Engineering, Bahria University, Islamabad, Pakistan. Fax: +92-51-9260885.
E-mail address: engr.taimoor@bui.edu.pk (T. Hassan).

http://dx.doi.org/10.1016/j.cmpb.2016.09.004
0169-2607/© 2016 Elsevier Ireland Ltd. All rights reserved.

1. Introduction

Macular diseases are the collective group of diseases that affect the central vision. If they are left untreated, they can cause severe visual impairments or even blindness. Unfortunately due to lack of health resources in developing countries like Pakistan, the rate of visually impaired people are increasing day by day [1]. Globally, macular diseases are the second major cause of blindness following cataract [2]. The most common macular diseases are macular edema (ME) and central serous retinopathy (CSR). ME occurs due to retinal swellings within macular pathology where these swellings are mainly due to diabetes and cataract surgeries [3]. CSR is another variation of macular disorders that damage the central vision of a person. CSR is due to the rapture in the retinal pigment epithelium (RPE) which leads to the accumulation of serous fluid beneath neurosensory retina [4,5]. Fig. 1 shows the OCT image of a healthy person and a patient with macular disorders where the foveal thickness between ILM and choroid is indicated for both cases.

A number of articles have presented detailed clinical literature on ME and CSR using OCT images. Shrestha et al. [6] found the usefulness of OCT imaging after ME surgeries. They consider a dataset of 60 patients in their study. Hannouche and Ávila [7] compared the different eye testing techniques and concluded that OCT imaging is more effective in early macular syndromes. Mokwa et al. [8] also compared different eye testing techniques for grading of age related macular degeneration (AMD) and choroidal neovascularization (CNV) and they concluded that OCT is more efficient than fundus fluorescein angiography (FFA) to diagnose early symptoms of macular pathology; however, it cannot fully replace FFA. Zhang et al. [9] gave an overview of OCT imaging system and also its usage for diagnosing and treating diabetic macular edema (DME). Ferrara et al. [10] used 15 eyes of 13 patients to extract different features of retinal pigment epithelium (RPE) and choroid to diagnose CSR positive candidates. Helmy and Allah [11] used the dataset of 104 eyes of 86 patients to detect cystoid macular edema (CME). The sample population was from the age group of 50 to 71 years. In their study, they concluded that OCT imaging is a very useful non-invasive technique to detect early pathological changes and cyst spaces within macula. Teke et al. [12] compared fundus auto fluorescence (FAF) and OCT imaging on a dataset of 100 CSR candidates and concluded that both techniques are quite effective in clinically diagnosing CSR. Wani et al. [13] used OCT and FFA to diagnose 48 CSR candidates and they concluded that OCT is the good alternative to fluorescein angiography (FA) for diagnosing CSR. Mitarai et al. [14] used a dataset of 26 patients with 23 to 3 men and women ratio and they have detected the variations in fluid leakage points in CSR candidates. Ahlers et al. [15] considered 18 patients suffering from CSR and they concluded that OCT gives an objective evaluation of retinal pathology under CSR symptoms. Apart from this, some researchers have also proposed automated algorithms to detect ME from OCT images. Zhang et al. [16] segmented retinal layers to diagnose CME from macular pathology using adaptive boosting (AdaBoost) algorithm and they achieved the accuracy of 98.60%. Wilkins et al. [17] used a dataset of 16 subjects and detected inter-retinal fluid by manually annotating inner limiting membrane (ILM) and retinal pigment epithelium (RPE) with the sensitivity and specificity ratings of 91% and 96% respectively. Srinivasan et al. [18] automatically diagnosed diabetic macular edema (DME), AMD and healthy pathology within macular region and they achieved the accuracy of 100%, 100% and 86.67% respectively. Sugruk et al. [19] proposed a fully automated method to diagnose AMD and DME. For AMD, they detect RPE abnormalities within macular scan and to detect DME, they extracted cyst segments with the accuracy of 100% and 86.6% respectively.

To the best of our knowledge, no technical paper related to automated detection of CSR was found in literature except Ref. [20] in which we proposed a structure tensor based automated detection of CSR, ME and healthy pathology from OCT B-scans. We achieved an overall accuracy of 98.88% for correctly classifying ME, CSR and healthy scans. Here, we propose an extension of the fully automated algorithm proposed in Ref. [20] to detect ME and CSR by reconstructing 3D retinal thickness surfaces and cyst cavity from OCT volumes. The robust reconstruction is based on adaptive de-noising filter [21] and coherent tensors. Afterwards the proposed system uses SVM to distinguish between healthy, CSR and ME subjects. The rest of the paper is organized as follow: section 2 is about the in-depth description of proposed methodology, section 3 demonstrates our results and accuracy for automatically classifying macular subjects, section 4 is about the discussion on our proposed implementation and section 5 outlines conclusions and future directions.

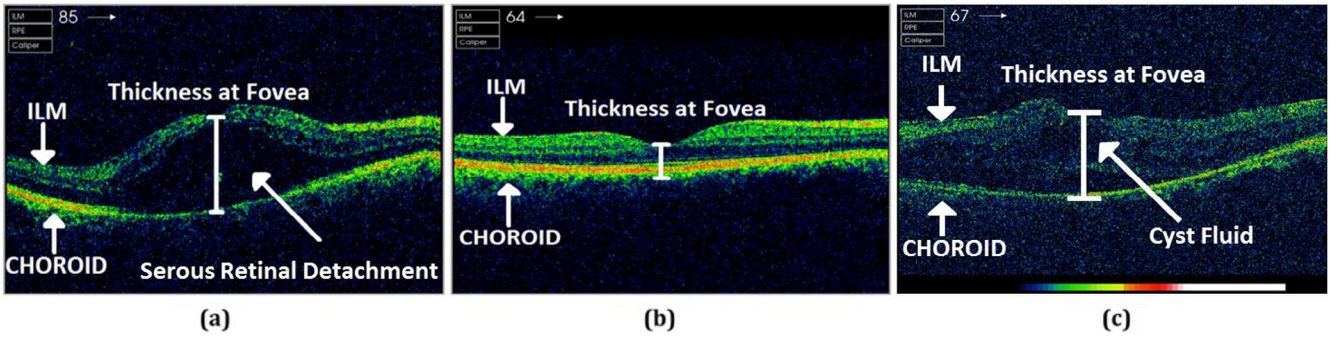

Fig. 1 – Macular analysis: (a) CSR affected OCT scan; (b) normal macular OCT scan; (c) ME affected OCT scan.

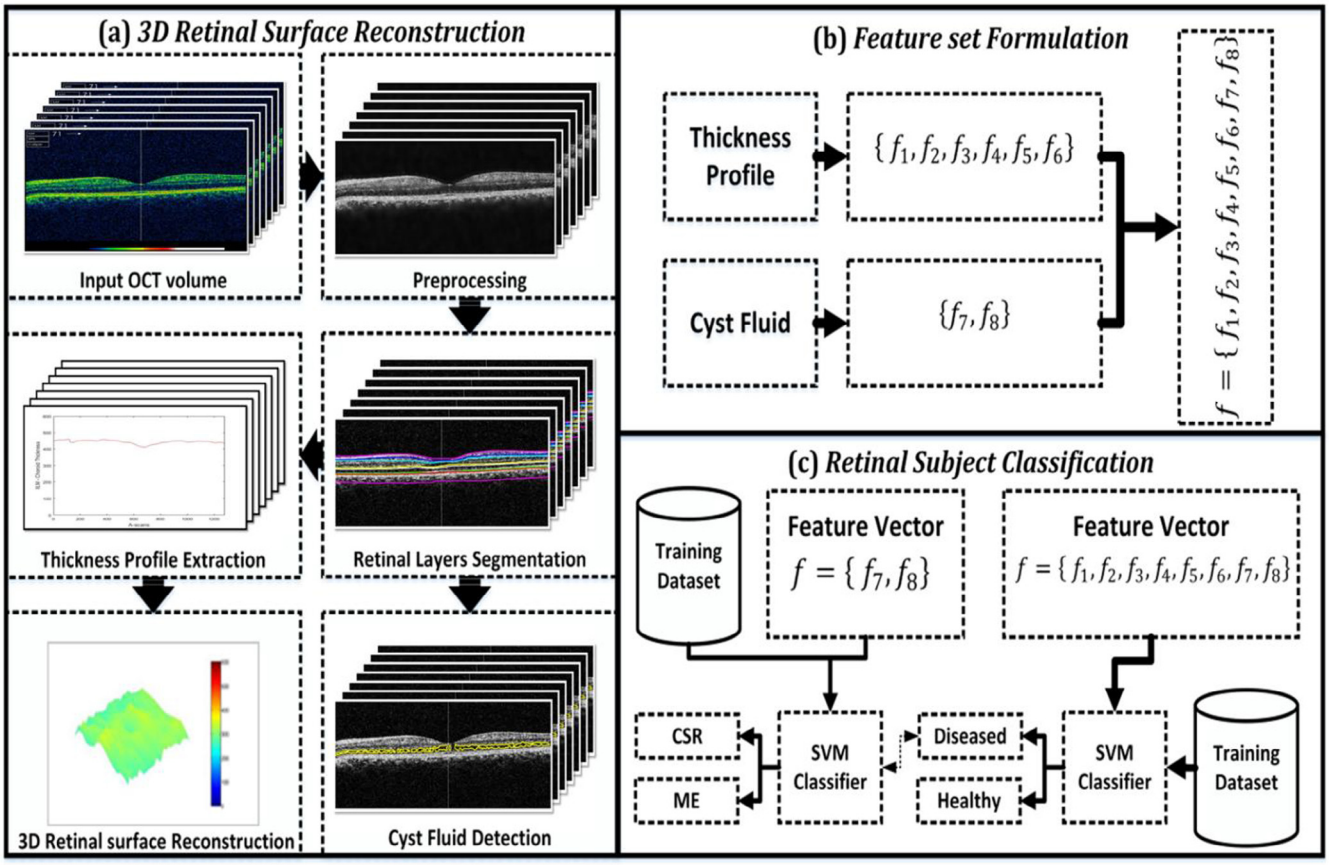

Fig. 2 – Proposed methodology: (a) 3D retinal surface reconstruction; (b) feature set formulation; (c) retinal subject classification.

2. Proposed methodology

The proposed algorithm for multi-classification of ME, CSR and healthy candidates is based on three stages. The first stage is related to the robust reconstruction of 3D retinal thickness surfaces and cyst space cavities from input OCT B-scan volume which are fed to the second stage in which 8D feature vector is extracted. The 8D feature vector "*f*" is composed of 8 distinctive features from all the three thickness sides (axis) of 3D surface and cyst space cavity which are then passed to the third stage. The third stage is related to the supervised multi-classification of ME, CSR and healthy cases using trained pair of SVM classifiers. The classification is based on the passed feature vector "*f*" upon which SVM was trained using 30 labeled volumes. The block diagram of the proposed system is shown in Fig. 2.

2.1. *OCT dataset acquisition*

The dataset which have been used in this article is collected locally from Armed Forces Institute of Ophthalmology (AFIO), Rawalpindi. The dataset has 90 OCT volumes (consisting of 128 B-scans) of 73 patients in which 54 were male and 19 were female. The OCT volumes within the dataset consist of time domain OCT (TD-OCT) B-scans which are acquired using TOPCON 3D OCT-2000 machine. The detailed description about the dataset is shown in Table 1.

Table 1 – Patients data and scanning parameters of OCT dataset.

Patients data		Scanning parameters	Type		
			Healthy	CSR	ME
Total patients	73	Total subjects	30	30	30
Male	54	Axial resolution (μm)	3 ~ 3.8	3 ~ 3.8	3 ~ 3.8
Female	19	Lateral resolution (μm)	11 ~ 13	7 ~ 13	11 ~ 13
Mean age	36.2	Azimuthal resolution (μm)	49 ~ 122	58 ~ 129	63 ~ 186
Total eyes	90	Scan resolution (pixel × pixel)	480 × 1280	480 × 1280	480 × 1280
Unilateral	56	B-scans	128	115 ~ 134	117 ~ 126
Bilateral	17	A-scans (points)	480 points	480 points	480 points

2.2. 3D retinal surface reconstruction

The first stage of our proposed algorithm is the reconstruction of 3D retinal surfaces and cyst spaces. Many automated methods are used to predict the retinal edema from best selected OCT B-scans; however, single B-scan is not enough to fully analyze retinal edema. In fact ophthalmologists also analyze the 3D retinal surface for objective evaluation of retinal pathology. Currently to the best of our knowledge, no automated method exists that incorporate reconstruction of 3D OCT surfaces for the diagnosis of macular edema and central serous retinopathy. Therefore we have extended our algorithm proposed in Ref. [20] to reconstruct accurate retinal and cyst surfaces which are then used for the automated diagnosis of ME, CSR and healthy candidates. The detailed description of each processing step to generate B-scan thickness profile from each frame has been already explained in Ref. [20] and here we will only discuss the extension of our algorithm to reconstruct and incorporate 3D retinal surfaces for the automated diagnosis of all the three types of retinal pathologies. After generating the thickness profile from the coherent tensor of each frame, a retinal surface $R(x, y, z)$ is reconstructed by combining them all into a single volumetric surface as shown in Fig. 3.

$R(x, y, z)$ is then smoothen using multivariate Gaussian smoothing filter as expressed in Eq. (1)

$$R_D(x, y, z) = \sum_{x_i \in w_x} \sum_{y_j \in w_j} \sum_{z_k \in w_k} \Delta * R(x_i, y_j, z_k) \tag{1}$$

where

$$\Delta = \frac{1}{\sqrt{(2\pi)^3 |\epsilon|}} e^{\left(-\frac{1}{2}(x-\mu)^T \epsilon^{-1}(x-\mu)\right)} \tag{2}$$

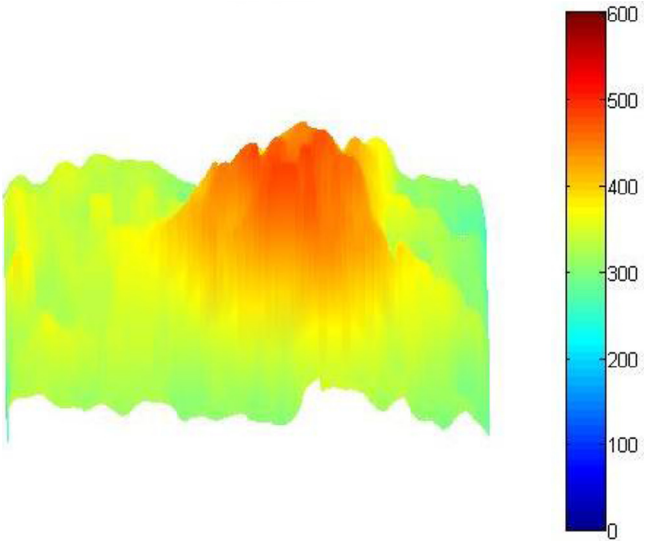

Fig. 3 – Reconstructed 3D retinal surface: cyst regions are highlighted in red color while normal regions are shown in green color. (For interpretation of the references to color in this figure legend, the reader is referred to the web version of this article.)

μ is the mean value of the neighboring Gaussian window and ϵ is the 3×3 covariance matrix.

2.3. Feature set extraction

After the successful reconstruction of 3D retinal surfaces, 8 distinct features are automatically extracted from retinal and cyst surfaces to classify healthy, CSR or ME pathology. 6 features are obtained from thickness surface generated from segmented ILM and choroid layer and 2 features are extracted from cyst fluid present within diseased retinal layers to form feature vector ($f = \{f_1, f_2, f_3, f_4, f_5, f_6, f_7, f_8\}$). The retinal surface has three axes or sides as shown in Fig. 4; the retinal surface is generated by taking the absolute difference of ILM and choroid in each B-scan frame.

The description of each feature to is given below:

Max thickness of left side (f_1): It is the maximum value in the mean thickness vector $T_{left}n(v)$, which is generated by taking the mean of the left side. f_1 is expressed by Eqs. (5–6) and $T_{left}n(v)$ is generated using Eqs. (3–4):

$$T_{left}n(v) = [T_{left}n(v_1), T_{left}n(v_2), \ldots, T_{left}n(v_i)] \tag{3}$$

where

$$T_{left}n(v_i) = (Mean|B_{ILMLeft}(u, v) - B_{ChoroidLeft}(u, v)|) \tag{4}$$

$$f_1 = max[T_{left}n(v)] \tag{5}$$

$$f_1 = max[Mean|B_{ILMLeft}(u, v) - B_{ChoroidLeft}(u, v)|] \tag{6}$$

Min thickness of the left side (f_2): It is the minimum value in the mean thickness vector $T_{left}n(v)$ which is due to minimum gap in $T_{left}n(v)$ as expressed by Eqs. (7–8):

$$f_2 = min[T_{left}n(v)] \tag{7}$$

$$f_2 = min[Mean|B_{ILMLeft}(u, v) - B_{ChoroidLeft}(u, v)|] \tag{8}$$

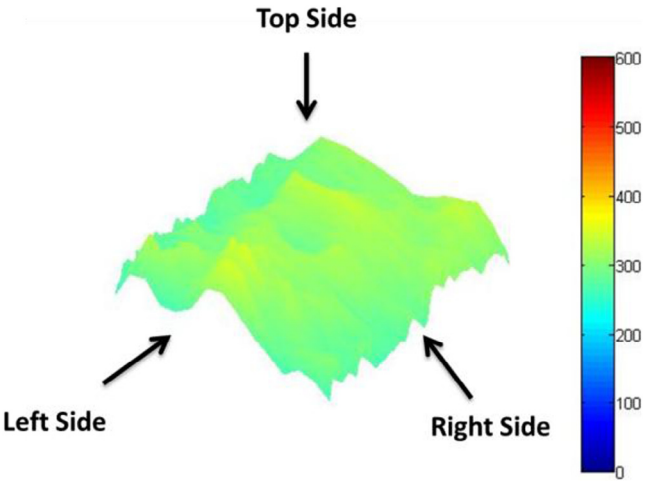

Fig. 4 – Three sides of reconstructed retinal surface.

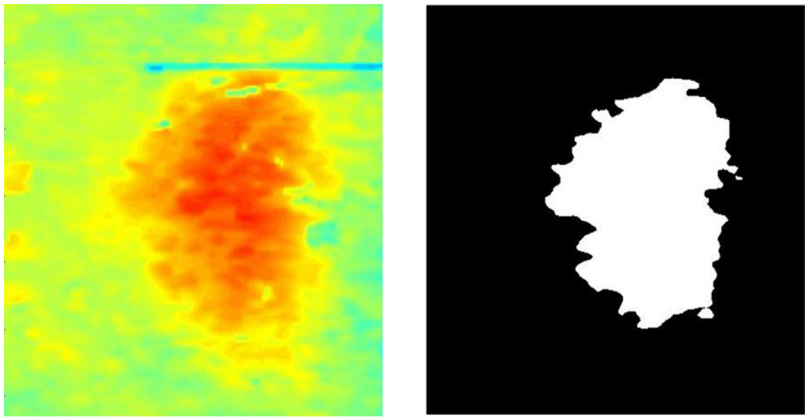

Fig. 5 – Retinal surface: (a) top projection; (b) binary map of (a).

Thickness variation in the left side (f_3): It is the absolute difference between f_2 and f_1 as expressed by Eq. (9), it tells about the variation between the layers due to presence of cyst fluid between the retinal layers.

$$f_3 = |f_2 - f_1| \tag{9}$$

Max thickness of right side (f_4): It is the maximum value in the mean thickness vector $T_{right}n(v)$, which is generated by taking the mean of the right side.

Min thickness of right side (f_5): It is the minimum value in the mean thickness vector $T_{right}n(v)$, which is due to minimum gap in $T_{right}n(v)$.

Thickness variation in the right side (f_6): It is the absolute difference between f_5 and f_4, which depicts the variation between retinal layers due to presence of cyst fluid.

Retinal Top Surface Area (f_7): The top surface area determines the area occupied by the leaked fluid within retinal layers. It is computed by taking area of top surface projection of $R(x, y, z)$ as expressed by the Eq. (10):

$$f_7 = TopSurfaceArea(R(x, y, z)) \tag{10}$$

Top surface area is computed by generating the binary map of $R(x, y, z)$ and computing the area of the binary map as shown in Fig. 5.

Cyst Energy (f_8): It is the total energy of a mean cyst space cavity calculated by Eq. (11). The block diagram of cyst energy extraction is also shown in Fig. 6. The purpose of calculating cyst energy is to discriminate ME cyst pathology from retinal serous pathology:

$$f_8 = |Low\ band(DWT(Mean(Cyst(x, y, z))))|^2 \tag{11}$$

The feature vector of five randomly selected samples from the unlabeled dataset is shown in Table 2. These vectors are generated for all the three types of macular pathologies. From Table 2, it can be observed that all the 8 features are quite distinct for all three cases.

2.4. *Classification*

The third stage of the proposed system is related to the classification of retinal pathology based on the extracted feature set. The proposed system is based on multi-level classification in which we have used pair of supervised SVM classifiers to classify all the three types of retinal pathology. At first the SVM was trained to classify healthy or diseased surface based on 8 extracted features, afterwards if the surface is classified as diseased, then it is further classified as CSR or ME based on 7th and 8th features. The classification process is also shown in Fig. 7.

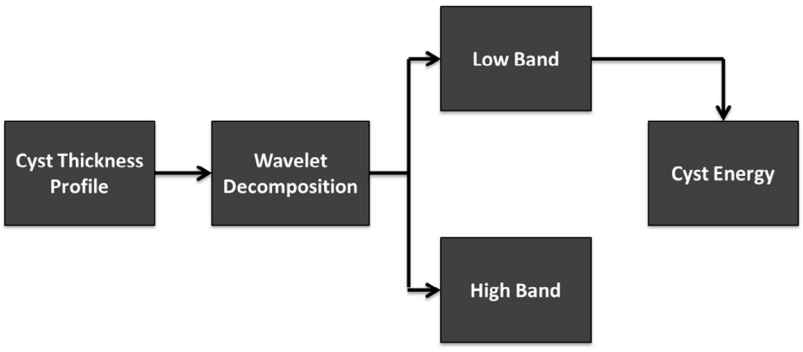

Fig. 6 – Cyst energy extraction through wavelet decomposition.

Table 2 – Features extracted from all 3 types of retinal subjects.

Type	Cases	Features							
		F1 (mm)	F2 (mm)	F3 (mm)	F4 (mm)	F5 (mm)	F6 (mm)	F7 (pixels)	F8 (volts^2.sec)
ME	Case 1	379.04	89.62	289.42	355.01	213.22	141.78	2654.60	89,855.1
	Case 2	369.83	212.67	157.16	407.20	241.07	166.13	2901.20	179,977
	Case 3	331.43	193.21	138.22	347.08	196.21	150.86	2937.77	138,123
	Case 4	350.21	160.24	189.97	350.49	199.54	150.95	3024.57	235,713
	Case 5	335.52	170.63	164.89	341.52	205.14	136.38	2859.13	152,351
	Mean	353.20	165.27	187.93	360.26	211.03	149.22	2875.45	159,203
	S.D.	20.855	46.915	59.693	26.698	17.982	11.312	137.681	53,818.6
CSR	Case 1	317.34	126.50	190.84	340.97	147.28	193.69	242.0	3423
	Case 2	342.87	104.62	238.24	376.75	193.15	183.60	755.3	3483
	Case 3	355.15	199.87	155.28	300.75	228.43	72.320	84.56	7182
	Case 4	330.47	150.58	179.89	346.58	176.98	169.60	96.84	5147
	Case 5	336.70	143.98	192.72	403.22	163.87	239.35	119.0	3398
	Mean	336.50	145.11	191.39	353.65	181.94	171.71	259.54	4526.6
	S.D.	14.070	35.410	30.137	38.729	30.981	61.405	284.13	1659.57
Healthy	Case 1	85.45	32.97	52.48	52.23	36.25	15.98	35	504.25
	Case 2	42.79	37.84	4.950	68.42	45.66	22.76	47	401.75
	Case 3	57.41	24.31	33.10	59.48	41.96	17.52	40	632.21
	Case 4	58.79	30.54	28.25	75.18	44.25	30.93	26	458.94
	Case 5	60.87	42.15	18.72	45.62	24.59	21.03	49	215.16
	Mean	61.06	33.56	27.50	60.18	38.54	21.64	39.40	442.46
	S.D.	15.38	6.839	17.61	11.92	8.585	5.851	9.343	152.82

2.4.1. *Classifier training phase*

For classification of retinal pathologies, we have used supervised support vector machines (SVM) classifier. After extracting 8 distinct features from retinal thickness and cyst surface, they are used to predict the respective retinal pathology. SVM is one of the most popular and widely used classifier [22], and two kernels multilayer perceptron kernel (MLP) and Gaussian radial basis function (RBF) are used in the proposed system. Training phase of classifier is shown in Fig. 8.

We used a total of 30 labeled OCT volumes (10 Healthy, 10 CSR, 10 ME) annotated by an expert ophthalmologist for training purpose of SVM classifiers. After computing the feature set "*f*," it is passed to supervised SVM classifiers. After classifying the labeled samples, K-fold cross validation is performed for different values of "K" to calculate maximum accuracy as shown in Table 3.

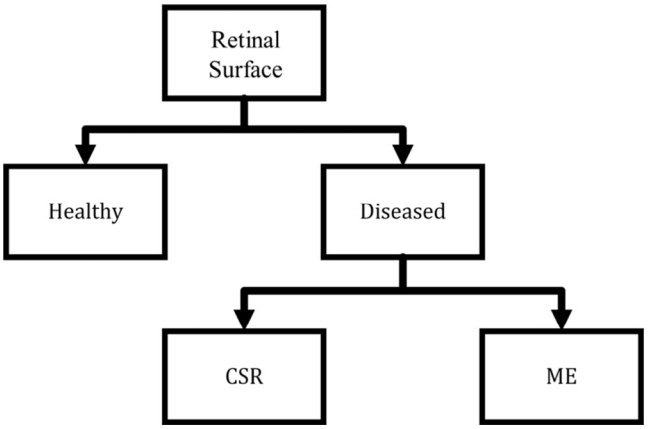

Fig. 7 – Multilevel supervised classification.

2.4.2. *Retinal subjects classification*

After training the classifier, it was used to classify test OCT volumes by extracting the 8D feature vector. The classification is based on multilevel as shown in Fig. 7 and the candidate volume is classified into one of the three cases i.e. healthy, ME positive or CSR positive. The flow chart of the proposed system is shown in Fig. 9.

3. Results

Different unlabeled OCT volumes from our dataset are passed to the proposed system for the automated diagnosis of macular syndromes and our system correctly classified all the ME and CSR candidates. For the healthy case, our proposed system correctly classified 29/30 subjects. These results on unlabeled dataset were also cross validated and verified by expert ophthalmologists. Table 4 shows the results of our proposed system for each type of pathology.

Fig. 10 shows the results of our cyst segmentation on randomly selected B-scan from each syndrome. Segmented ILM layer and choroid are shown in "red" and "green" color respectively, whereas segmented cysts are shown in "yellow" color.

Table 3 – Classifier cross validation performance.

K	Max accuracy
2	0.942
4	0.957
8	0.968
10	**0.980**
12	0.974

The bold row indicates the highest accuracy that has been achieved on the training dataset for K = 10.

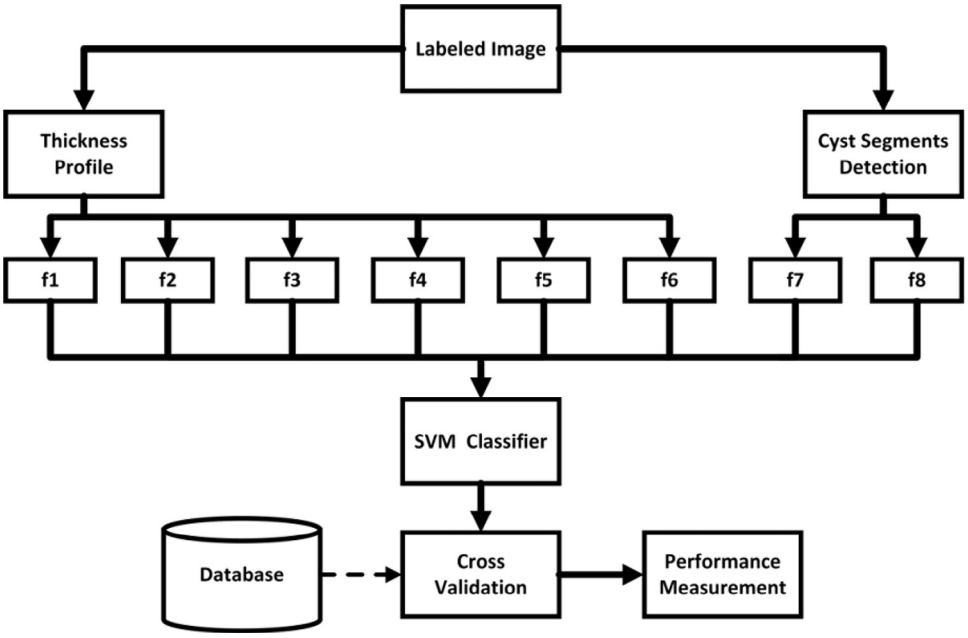

Fig. 8 – Training phase of SVM supervised classifier.

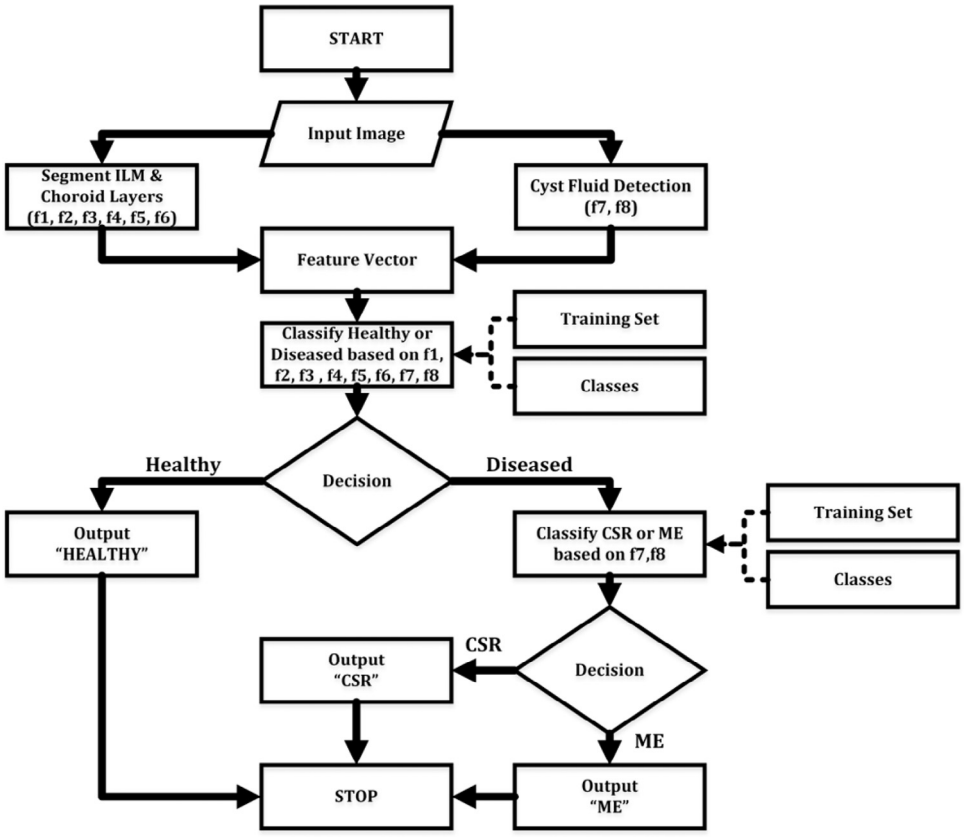

Fig. 9 – Flowchart of classification algorithm.

Table 4 – Achieved results.

Type	Correctly classified	Accuracy	Sensitivity	Specificity
Healthy	29/30	98.88%	100%	96.66%
CSR	30/30			
ME	30/30			

Some of the randomly selected retinal surfaces for all the three types of retinal pathologies are shown in Fig. 11. The peak thickness is defined by red color and the dip is defined by the blue color.

4. Discussion

This paper proposes an automated method for diagnosing three types of macular pathologies (i.e. ME, CSR and healthy) from OCT volumes. We have extended our algorithm proposed in Ref. [20] to incorporate 3D retinal surfaces to diagnose all the three types of macular syndromes since a single B-scan cannot be used to diagnose the severity of the disease. The dataset used in this research is collected from AFIO and it contains 90 OCT volumes (30 CSR, 30 ME and 30 healthy volumes). The detailed description about the dataset is presented in Table 1. The proposed system takes an OCT volume as an input and reconstruct 3D retinal surface by extracting a coherent tensor from each B-scan. The proposed system also extracts cyst segments from each scan and generates a cyst surface. Then both of these surfaces are used to extract 8D feature vector which is passed to multilevel SVM classifiers to classify all the three cases. The proposed method is quite fast and robust in detecting macular pathologies. It takes around a minute on average to reconstruct retinal surfaces and diagnose a candidate volume, on a machine with core i5 (2.2 GHz) 5th generation multithreaded processor and 4 GB RAM. Apart from this, the proposed system is rotation invariant and it incorporates the full 3D OCT volume instead of single best selected B-scan, so the proposed system can objectively evaluate the retinal pathology which can be easily cross validated and verified by ophthalmologist. 3D retinal thickness surface provides the best and objective method to detect any type of retinal pathology and the proposed system reconstructs those surfaces to automatically diagnose CSR, ME and healthy subjects. The dataset used in this research was annotated by multiple expert ophthalmologists and our system correctly classified all the diseased subjects. Our proposed system is dependent on the quality of the input scans as there were some poor scans in our dataset and one of such scans led to the misclassification of healthy candidate as false positive. Fig. 12 depicts two of such low quality B-scans and we can see that the significant portion of neurosensory retina is washed out in these B-scans.

Since there is a tradeoff between sensitivity and specificity, we have tuned our proposed system to give more priority to the diseased volumes as compared to the healthy ones because false negatives are more critical in this application as compared to the false positives. The proposed technique can act as an aid to ophthalmologists. A machine can automatically reconstruct 3D retinal surfaces and can measure the retinal thickness, which doctors can use to back their decision. The proposed system can help in clinical studies as a decision support system and fresh doctors with less experience can rely on this.

5. Conclusion

An automated algorithm is proposed here which is used to diagnose three types of macular pathologies. The proposed system is based on OCT volume from which 3D retinal surfaces are reconstructed by extracting a coherent tensor from each B-scan.

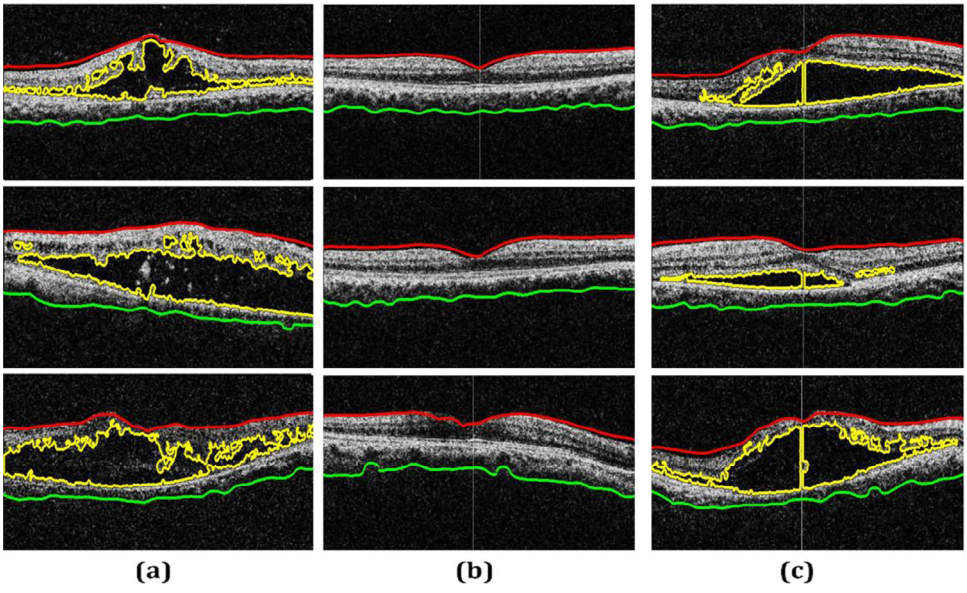

Fig. 10 – Unlabeled images: (a) ME cyst, ILM and choroid segmentation; (b) healthy segmentation; (c) CSR cyst, ILM and choroid segmentation.

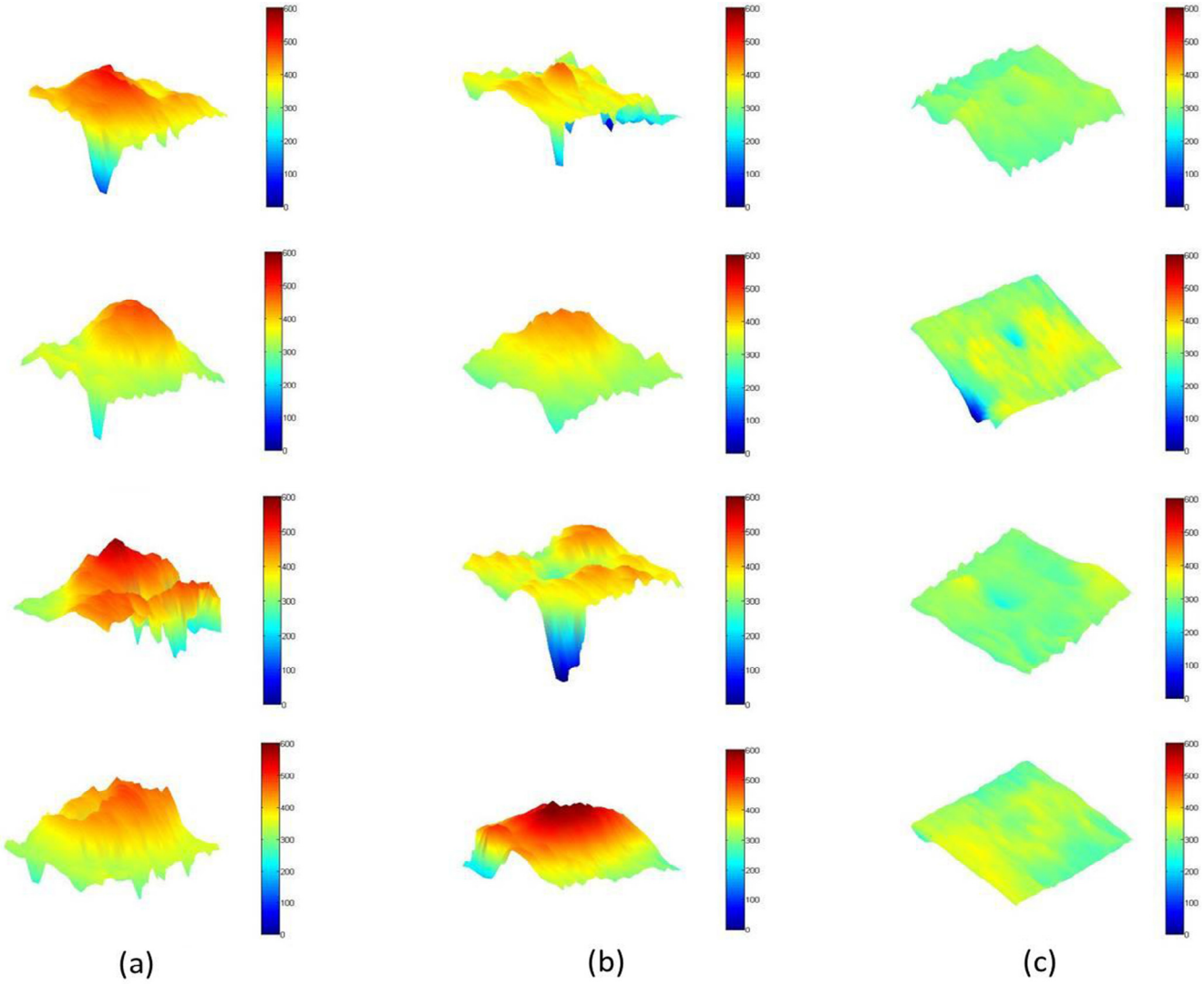

Fig. 11 – 3D retinal thickness surfaces: (a) ME classified surfaces; (b) CSR classified surfaces; (c) healthy surfaces.

The proposed system uses a supervised SVM based multi-level classification system as shown in Fig. 7. The dataset used in this research has been collected from AFIO and the detailed information about the dataset is presented in Table 1.

Also, our system is quite fast, robust and has promising receiver operator characteristics (ROC) ratings. Currently we have generated retinal surfaces (from 128 B-scans volumes) using a single thread sequential process and reconstructing retinal surfaces from a very large volume can be cumbersome. So in the future this can be optimized by processing each B-scan in parallel on multiple CPU or GPU threads. Also, this work can be extended for grading of these retinal diseases and the proposed method can be extended to diagnose other macular and ocular disorders such as AMD and glaucoma etc. The same system can be extended and tailored for circular optic nerve head (ONH) scans for diagnosis of glaucoma.

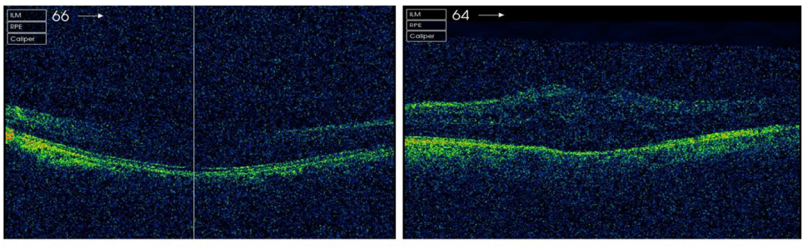

Fig. 12 – Bad quality OCT scans: (a) healthy; (b) diseased.

Acknowledgment

This research was supported by National ICT R&D Fund, and medical expertise for annotation and validation of data is provided by AFIO and Yusra Medical College, Islamabad Pakistan.

REFERENCES

[1] Z.H. Awan, P.S. Mahar, M.S. Memon, Blindness and poverty, Pak. J. Ophthalmol. 27 (2011) 165–170.
[2] A. Khan, Q. Riaz, F. Soomro, U. Qidwai, U. Qazi, Frequency and patterns of eye diseases in retina clinic of a tertiary care hospital in Karachi, Pak. J. Ophthalmol. 27 (2011) 155–159.
[3] L. Conceicao, I. Pires, J.C. Vaz, Diabetic macular edema, Chapter 1, in: Optical Coherence Tomography, Springer-Verlag Heidelberg, 2012. http://dx.doi.org/10.1007/978-3-642-27410-7.
[4] F.E. Hirai, M.D. Knudtson, B.E.K. Klein, R. Klein, Clinically significant macular edema and survival in type 1 and type 2 diabetes, Am. J. Ophthalmol. 145 (4) (2009) 700–706.
[5] N. Vukojevic, J. Sikic, D. Katusic, B. Saric, Types of central serous retinopathy, analysis of shape, topographic distribution and number of leakage sites, Coll. Antropol. 25 (2001) 83–87.
[6] A. Shrestha, N. Maharjan, A. Shrestha, R. Thapa, G. Poudyal, Optical Coherence Tomographic assessment of macular thickness and morphological patterns in diabetic macular edema: prognosis after modified grid photocoagulation, Nepal J. Ophthalmol. 4 (2012) 128–133.
[7] R.Z. Hannouche, M.P. Ávila, Detection of diabetic foveal edema with bio microscopy, fluorescein angiography and Optical Coherence Tomography, Arq. Bras. Oftalmol. 71 (2008) 759–763.
[8] N.F. Mokwa, T. Ristau, P.A. Keane, B. Kirchhoff, S.R. Sadda, S. Liakopoulos, Grading of age-related macular degeneration: comparison between color fundus photography, fluorescein angiography, and spectral domain Optical Coherence Tomography, J. Ophthalmol. 4 (2013) 1–6.
[9] W. Zhang, K. Yamamoto, S. Hori, Optical Coherence Tomography for assessment of diabetic macular edema, Int. J. Ophthalmol. 1 (2008) 370–373.
[10] D. Ferrara, K.J. Mohler, N. Waheed, M. Adhi, J.J. Liu, I. Grulkowski, et al., En face enhanced-depth swept-source Optical Coherence Tomography features of chronic central serous chorioretinopathy, Ophthalmology 121 (2014) 719–726.
[11] Y.M. Helmy, H.R.A. Allah, Optical Coherence Tomography classification of diabetic cystoid macular edema, Clin. Ophthalmol. 13 (2013) 1731–1737.
[12] M.Y. Teke, U. Elgin, P.N. Yuksekkaya, E. Sen, P. Ozdal, F. Ozturk, Comparison of autofluorescence and Optical Coherence Tomography findings in acute and chronic central serous chorioretinopathy, Int. J. Ophthalmol. 7 (2014) 350–354.
[13] J.S. Wani, P.A. Bhat, A. Ahangar, S. Ismail, Role of Optical Coherence Tomography in central serous chorioretinopathy, J. Evol. Med. Dent. Sci. 45 (2015) 7801–7809.
[14] K. Mitarai, F. Gomi, Y. Tano, Three-dimensional optical coherence tomographic findings in central serous chorioretinopathy, Graefes Arch. Clin. Exp. Ophthalmol. 244 (2006) 1415–1420.
[15] C. Ahlers, W. Geitzenauer, G. Stock, I. Golbaz, U.S. Erfurth, C. Prunte, Alterations of intraretinal layers in acute central serous chorioretinopathy, Acta Ophthalmol. 87 (2009) 211–216.
[16] L. Zhang, W. Zhu, F. Shi, H. Chen, X. Chen, Automated segmentation of intraretinal cystoid macular edema for retinal 3D OCT images with macular hole, Proc. IEEE Int. Symp. Biomed. Imaging 12 (2015) 1494–1497.
[17] G.R. Wilkins, O.M. Houghton, A.L. Oldenburg, Automated segmentation of intraretinal cystoid fluid in Optical Coherence Tomography, IEEE Trans. Biomed. Eng. 59 (4) (2012) 1109–1114.
[18] P.P. Srinivasan, L.A. Kim, P.S. Mettu, S.W. Cousins, G.M. Comer, J.A. Izatt, et al., Fully automated detection of diabetic macular edema and dry age-related macular degeneration from optical coherence tomography images, Biomed. Opt. Express 5 (2014) 3568–3577.
[19] J. Sugruk, S. Kiattisin, A.L. Lasantitham, Automated classification between age-related macular degeneration and diabetic macular edema in OCT image using image segmentation, in: IEEE Biomedical Engineering International Conference, 2014.
[20] B. Hassan, G. Raja, T. Hassan, M.U. Akram, Structure tensor based automated detection of macular edema and central serous retinopathy using optical coherence tomography images, J. Opt. Soc. Am. A. Opt Image Sci Vis. 33 (2016) 455–463.
[21] S. Kockanat, N. Karaboga, A novel 2D-ABC adaptive filter algorithm: a comparative study, Digit. Signal Process. 40 (2015) 140–153.
[22] R.E. Fan, K.W. Chang, C.J. Hsieh, X.R. Wang, C.J. Lin, LIBLINEAR: a library for large linear classification, J. Mach. Learn. Res. 9 (2008) 1871–1874.